RSC Advances

ROYAL SOCIETY OF CHEMISTRY

www.rsc.org/advances

RSC Advances

RSCPublishing

PAPER

Tunable Dielectric Constant of Polyimide-Barium Titanate Nanocomposite Materials as the Gate Dielectrics for Organic Thin Film Transistors Applications†

Cite this: DOI: 10.1039/x0xx00000x

Received 00th January 2012,
Accepted 00th January 2012

DOI: 10.1039/x0xx00000x

www.rsc.org/

Yang-Yen Yu,[abc*] Cheng-Liang Liu,[d*] Yung-Chih Chen,[a] Yu-Cheng Chiu,[e] and Wen-Chang Chen[e]

We report on a systematic study of hydroxyl-containing polyimide (PI)-$BaTiO_3$ (BT) nanoparticles (NPs) nanocomposite dielectric materials, to determine the effects of BT NPs loadings (X) for X = 0, 2, 5, 8, 10, and 12 wt%, on p-type pentacene organic thin film transistors (OTFTs). A condensation reaction to produce well-dispersed BT NPs within the PI matrix was followed by spin-coating to form a dielectric thin film directly on a silicon substrate. The thermal, optical, surface, dielectric, and electrical properties of the **PI-BPX** hybrid dielectric composite correlated to BT content for each sample. The hybrid dielectric composites exhibit tunable insulating properties, including high dielectric constant values in the range 5.2~11.3, high capacitances from 3.1 to 27.9 nF cm^{-2} for a film thickness of approximately 350 nm, and low leakage current densities in the range of 1.85×10^{-7}~2.76×10^{-6} A cm^{-2} at 2 MV cm^{-1}. Bottom-gate top-contact OTFTs fabricated using various **PI-BPX** hybrid dielectrics, exhibit low threshold voltages of -4.09~2.62 V, moderately high field-effect mobility rates of 3.36×10^{-2}~2.32×10^{-1} cm^2 V^{-1} s^{-1}, and high ON/OFF ratios of approximately 10^5. This study opens a route towards transparent and highly stable hybrid dielectric materials with tunable dielectric properties, by careful selection of NPs and polymer matrix combinations.

Introduction

Organic thin film transistors (OTFTs) have attracted considerable attention for their unique features, including low fabrication cost, flexibility, and ease of processing in solution, compared to their inorganic counterparts.[1-7] Much research effort has been directed at modifying OTFTs structural design to improve their performance in organic and polymeric semiconductors.[8-10] Other approaches, such as controlling the deposition of crystalline organic films[11-13] and controlling the nature of the interfaces present[14-18] have also been developed.

In OTFTs, the interface between gate dielectric and organic semiconductor plays an important role, because charge transport is confined to a thin layer of the semiconductor close to this interface. Smoothing the dielectric surface by using a thin polymer dielectric layer can often reduce the numbers of surface traps, optimize organic semiconductor growth, and control its morphology. However, this approach has the disadvantages of reducing the dielectric constant, resulting in low capacitance and high leakage currents.[19-21]

Alternatively, a high dielectric constant material such as a metal oxide can induce a greater density of accumulated charge carriers in the channel region for a given electric field, but most of these are based on ceramic materials that generally require high temperature annealing processes and expensive deposition equipment.[19-21] Combining organic polymer and inorganic constituents to form a hybrid insulator are an attractive strategy that can provide excellent candidates for OTFTs gates.[21,22] The dielectric properties of hybrid dielectrics comprising mixtures of polymers and inorganic nanofillers, including nanoparticles (NPs), nanoclusters, and nanotubes, can be tuned by varying the type and concentration of nanofiller materials, such as by using different inorganic oxides.[23-43]

[a] Department of Materials Engineering, Ming Chi University of Technology, New Taipei City 24301, Taiwan. E-mail: yyyu@mail.mcut.edu.tw
[b] Battery Research Center of Green Energy, Ming Chi University of Technology, New Taipei City 24301, Taiwan.
[c] Center for Thin Film Technologies and Applications, Ming Chi University of Technology, New Taipei City 24301, Taiwan.
[d] Department of Chemical and Materials Engineering, National Central University, Taoyuan, 32001 Taiwan. E-mail: clliu@ncu.edu.tw
[e] Department of Chemical Engineering, National Taiwan University, Taipei, 10617 Taiwan.
† Electronic Supplementary Information (ESI) available. See DOI: 10.1039/b000000x/

Polyimide (PI) is an excellent insulating material for OTFTs applications, and provides good thermal and mechanical stability.[44-47] Barium titanate ($BaTiO_3$; BT) NPs have a large dielectric constant and behave similarly to ferroelectric dielectric materials. The production of polymer-BT NPs hybrid thin films by simple solution techniques provides high quality dielectric nanocomposite materials.[37,38] Polymer hybrids materials and their production method for the controlled synthesis of hybrid nanostructures were obtained from templating NPs dispersions in continuous polymeric matrix. Fine-tuning the electrical and morphological properties of gate dielectrics based on a stable PI matrix contained within high dielectric constant BT NPs can improve the performance of OTFTs devices.

To prepare solution-processable organic-inorganic hybrid gate dielectric materials for use in OTFTs devices, we synthesized and characterized a series of hybrid PI-BT nanoparticle (**PI-BTX**) based dielectrics, varying X (BT loading) as 0, 2, 5, 8, 10, and 12 wt% (Scheme 1). Well-dispersed BT NPs in a PI matrix were spin-coated to form hybrid dielectric films. Varying the concentration of BT NPs provides control over the dielectric properties and performance of the pentacene-based OTFTs. We show that these hybrid dielectrics are more electrically effective than neat PI (**PI-BT0**), and demonstrate the tailoring of dielectric properties through modification of the organic-inorganic composition. Our findings provide insight towards the development of stable transparent dielectric materials for future electronic applications.

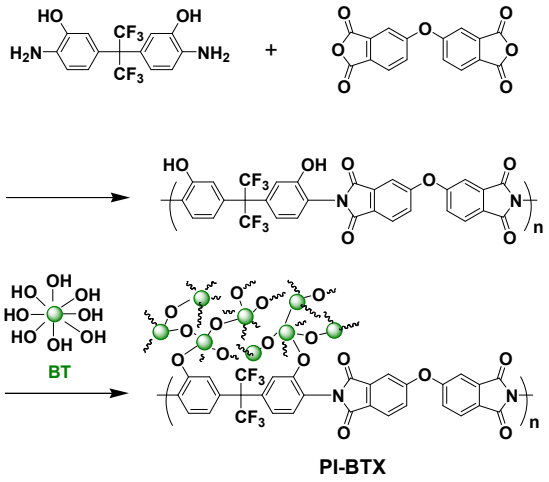

Scheme 1 Synthetic route for **PI-BTX** hybrid nanocomposite dielectric thin film.

Experimental

Materials

2,2-Bis(3-amino-4-hydroxyphenyl)hexafluoropropane (Matrix Scientific, 98%) and 4,4-oxydiphthalic anhydride (Aldrich, 97%), barium titanate ($BaTiO_3$, Seedchem Company PTY. LTD, 99%; particle size of ~30 nm) were used to prepare the **PI-BTX** hybrid dielectric films. All solvents, including isoquinoline (95%), tetrahydrofuran (THF, 99.9%), 1-methyl-2-pyrrolidinone (NMP, 99.9%), N,N'-dimethyl acetamide (DMAc, 99.5%), and toluene (99.8%) were provided by Tedia chemicals or Acros Organics. Pentacene, used as an organic semiconductor, was purchased from TCI Co. Ltd. All chemicals and solvents were used as received, without further purification.

General Procedures of Polymerization

Soluble PI was prepared by the imidization of a polyamic acid (PAA) solution. First, 2,2-bis(3-amino-4-hydroxyphenyl)hexafluoro propane (0.733 g) was placed into a 100 mL three-necked round-bottom flask under nitrogen, and then 8 mL of NMP and 0.476 mL of isoquinoline were added to dissolve the reagents. Next, 4,4-oxydiphthalic anhydride (0.620 g) was slowly added with vigorous stirring. The reaction mixture was stirred for 5 h at room temperature, and then toluene (2 mL) was added to the solution. The prepared PAA solution was thermally imidized at 150 °C for a further 18 h, and then cooledto room temperature. The homogeneous 2,2-bis(3-amino-4-hydroxyphenyl) hexafluoropropane and 4,4-oxydiphthalic anhydride solution was precipitated by the addition of 300 mL of methanol. A white-gray precipitate was recovered and subsequently dried in vacuo at 60 °C for 48 h (yield: 83%).[48,49]

Scheme 1 shows the general reaction scheme for the preparation of the **PI-BTX** hybrid solutions, where "**X**" is a number that refers to the weight percent of BT in the hybrid materials. Taking **PI-BT12** as an example, BT (0.0273 g) in 0.5 mL of DMAc was added into a 25 mL round-bottom flask. Then, PI (0.2 g) dissolved in 2 mL of DMAc was added drop wise to the solution by syringe, and the mixture stirred at room temperature for 30 min to obtain the **PI-BT12** hybrid solution. To prepare the **PI-BT12** hybrid thin film, the precursor **PI-BT12** solution was filtered and spin-coated onto a silicon wafer at 2000 rpm for 20 s. The resulting hybrid dielectric film was soft-baked at 60 °C for 20 min, 100 °C for 20 min, then at 150 °C for 1 h.

Characterization

Fourier transformed infrared (FTIR) spectra of the prepared **PI-BTX** hybrid thin films were acquired using on using a PerkinElmer Spectrum One spectrophotometer. In situ Raman spectroscopy was performed to determine and compare the phase transition temperatures using a Renishaw Inivia Raman microscope over a wavenumber range of 150~1000 cm^{-1} and temperature from 25 to 300 °C. The thermal properties of the **PI-BTX** hybrids were assessed using a TA Instruments Q50 thermogravimetric analysis (TGA) instrument and Q20/RSC90 differential scanning calorimeter (DSC) at heating rates of 20 and 10 °C min^{-1}, respectively. Contact-angle analysis was performed using an optical contact-angle apparatus with data acquisition software. The transmittances of the hybrid films coated on the quartz substrates were collected using a Jasco V-650 UV/Vis/NIR spectrophotometer. XRD analysis was performed on a PANalytical X' Pert PRO MPD X-ray diffractometer using CuKα radiation. The morphologies of thin films were observed by a high-resolution transmission electron microscope (HRTEM; JEOL, JEM-2100), a scanning electron microscope (SEM; Hitachi H-2400), and an atomic force microscope (AFM; Veeco DI 3100). The thicknesses of the **PI-BTX** hybrid thin films were analyzed by profilometry (ET-4000, Kosaka Laboratory Ltd).

OTFTs Fabrication and Characterization

OTFTs were fabricated on Si substrates using bottom-gate top-contact (BGTC) architecture. Heavily doped n^+ Si substrates were cleaned with deionized water, acetone, and isopropanol in an ultrasonic bath. After deposition of the hybrid dielectric layer (~350 nm), the pentacene active layer (~50 nm) was fabricated by thermal evaporation deposition at the pressure of approximately 10^{-7} Torr and deposition rate of 0.5 Å s^{-1}. Finally, Au source and drain electrodes were deposited on the active semiconducting layer by vacuum thermal evaporation, to provide source-drain contacts of length (L) = 50 μm and width (W) = 1000 μm. For the metal/insulator/metal (MIM) test structures, 0.6 mm diameter A1 electrodes were deposited directly onto the gate hybrid dielectric/Si films by shadow masking. MIM direct current measurements and OTFTs measurements were performed under ambient conditions using a probe station interface with an Agilent E4980A precision LCR meter (10 kHz to 1 MHz), and Agilent B1500A semiconductor device parameter analyzer.

Results and Discussion

PI-BTX hybrid dielectric film fabrication and characterization

The **PI-BTX** hybrid materials provided the gate dielectric for OTFTs devices. PI is well suited for use as the insulating matrix because of its high thermal and environmental stability and easy chemical modification. We performed two-step polymerization process of PI, involving polyamic acid synthesis and chemical imidization. Hybrid thin films were prepared by spin coating a solution of the appropriate precursor followed by thermal curing, as described in the Experimental section. Thermal treatment results in the formation of links between the prepared functionalized PI via its pendent hydroxyl groups, to the surface-modified BT NPs filler material. The dispersion and aggregation behaviors of the NPs determine the dielectric and film properties of **PI-BTX** hybrids. The combination of high dielectric constant guest fillers with a stable polymer host can provide solution-processable **PI-BTX** dielectric materials.

We studied the influence of composition on the structure and properties of dielectric films comprising a purely inorganic BT phase, polymeric material, and inorganic and polymer hybrid components, present in various weight ratios. Three main spectral features of BT ceramics detected by Raman spectroscopy (Fig. 1(a))at 25 °C are: (1) An intense broad band appearing at 508 cm^{-1} [A1 (TO)], (2) a broad, weak band at 711 cm^{-1} [A1 (LO)], and (3) a sharp band at 306 cm^{-1} [B1, E(TO+LO)], indicating that BT NPs possess coexisting rhombohedral and orthorhombic phases similar to that described in a previous report.[50] The structures of treated **PI-BTX** nanocomposite films were examined by a combination of Raman and FTIR spectroscopies. Fig. 1(a) shows Raman spectra of pure BT, PI (**PI-BT0**) and several **PI-BTX** hybrids (**PI-BT2**, **PI-BT5**, **PI-BT8**, **PI-BT10**, and **PI-BT12**). The three main BT absorption bands were also present in the spectra of the **PI-BTX** hybrids. The intensity of these characteristic BT bands increases with BT concentration. Fig. 1(b) and Fig. S1 of ESI† show the FTIR spectra for pure BT and for **PI-BTX** hybrids with various compositions, respectively. Pure PI (**PI-BT0**) is identifiable during the complete PAA polycyclic-dehydration process, by imide C=O stretching bands at 1788 cm^{-1} and a C-N-C stretching absorption at 1370 cm^{-1} and absence of C=O from amid acid at 1680 cm^{-1}. The intense

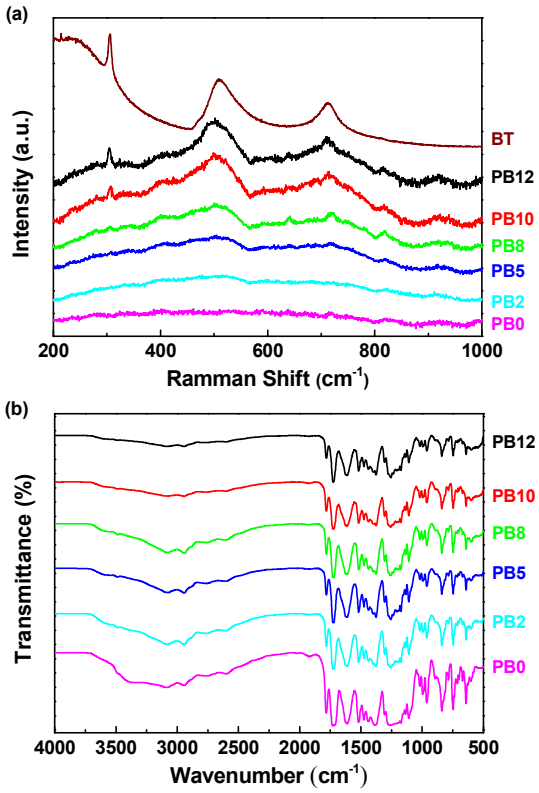

Fig. 1. (a) Raman spectra and (b) FTIR spectra of **PI-BTX** hybrid nancomposite thin films.

peaks around 3000 cm^{-1} are attributed to the hydroxyl (-OH)stretching from the side chain of PI, and the intensity of this band is slightly decreased in FTIR spectra when more BT NPs are covalently bonded with PI (from **PI-BT0** to **PI-BT12**). The strong and broad absorption band at approximately 500~700 cm^{-1} in both figures arises from Ti-O stretching vibrations in BT NPs. The **PI-BTX** hybrid FTIR spectra are consistent with the presence of both rhombohedral and orthorhombic morphologies. The greater the ratio of the BT in the hybrid sample, the greater the intensity of the Ti-O band appears in the low wavenumber region (500~700 cm^{-1}). The intensity of both Raman and FTIR spectra is proportional in part, to the number of contributing bonds present, thus, these spectra indicate that the introduction of BT nanofillers into the PI matrix results in the formation of **PI-BTX** hybrids. This

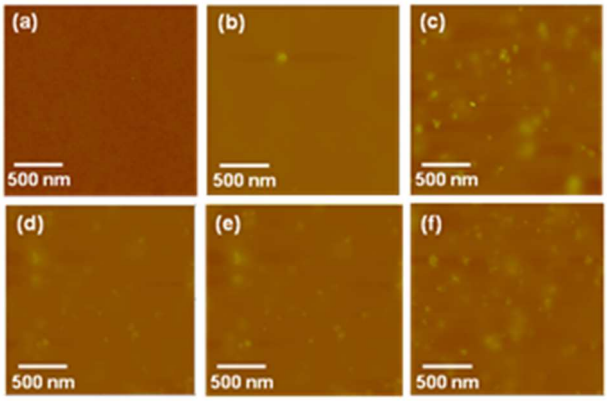

Fig. 2. AFM images dielectric surfaces: (a) **PI-BT0**, (b) **PI-BT2**, (c) **PI-BT5**, (d) **PI-BT8**, (e) **PI-BT10**, and (f) **PI-BT12**.

evidence also supports the proposed hybrid formation process, in which increases in the numbers of BT moieties in the system results in larger and more numerous BT regions.

The SEM image in Fig. S2 of ESI† and the AFM image in Fig. 2 show that spin coating of PI and BT NPs mixtures produce smooth and robust **PI-BTX** dielectric films at low temperature. SEM imaging of the hybrid surface demonstrates that the binding compatibility between PI and BT NPs on Si substrate facilitates the formation of uniform large-scale thin films with homogenous NP distributions, in OTFTs dielectric materials. The tapping-mode AFM height image of the dielectric layer (Fig. 2) reveals that the root-mean-square (rms) roughness values for 2 × 2 μm regions in the **PI-BTX** dielectric are in the range 0.475~11.924 nm. These AFM images of the hybrid **PI-BTX** samples show how surface morphology depends on the theoretical BT loading content in the hybrid material. Increases in the BT content of the PI matrix appears to result in increased surface rms roughness. However, all of the hybrid dielectric samples presented pinhole-free surfaces. Overall, our observations suggest that BT nanoparticles effectively disperse in the hybrid dielectric film PI matrix.

The XRD results (Fig. 3) for the sintered BT sample show the formation of a BT perovskite phase. We assigned the sharp X-ray reflections at 2θ = 23.6°, 32.7°, 40.5°, 46.1°, 52.3°, and 56.5° to (100), (110), (111), (200), (210) and (211) planes, respectively.[51] No other diffraction peaks related to BT or significant crystalline phases were present. With the exception of **PI-BT12**, the **PI-BTX** thin films only produced broad bands in the XRD spectra, indicating an amorphous structure for BT loadings up to 10%, regardless of the BT hybrid precursor **BTX** hybrid mixtures, as determined by TGA and DSC. All the thermal properties were summarized in Table 1. The content. Fig. S3 of ESI† shows the thermal behaviors of **PI-**decomposition temperature, defined as the temperature at which 5% loss of mass occurs, increases with increasing BT loading content. For pure PI (**PI-BT0**) and low BT concentrations (**PI-BT2**), we attributed the abrupt weight loss to a hydroxyl group, which remained unreacted during the condensation process at low BT content. A degradation observed at approximately 500 °C results from decomposition of the aromatic PI moiety. Sample residues seen in the high temperature region (approx. 800 °C) correlate linearly with the amount of BT incorporated within the PI matrix. The addition of inorganic BT enhances the composite material's thermal stability, for both decomposition temperature and glass transition temperature, suggesting that presence of the inorganic component limits segmental motion, by forming O-BT-O bonds.

Fig. 4 shows the transmittances of coated hybrid dielectric films over the entire visible region. Even at high BT loading concentration, all of the PI-BTX hybrid dielectric materials exhibit good transmittance (greater than 85% at 500 nm), and are colorless. These properties are beneficial for applications that require transparency such as by a transistors passivation layer used in a high resolution and brightness electronic display. The superior transparency of the **PI-BTX** hybrid may result from the reduced formation of charge transfer complexes, and limited electronic conjugation along the PI backbone, that arise from the presence of fluorine moieties, the non-coplanar PI geometry, and from the bulky BT substituents present in PI the side chains.[52]

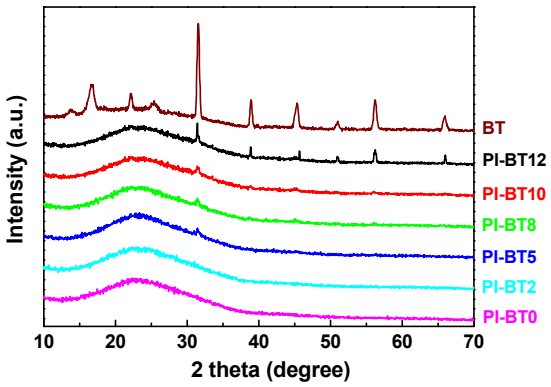

Fig. 3. XRD result for BT and **PI-BTX** samples.

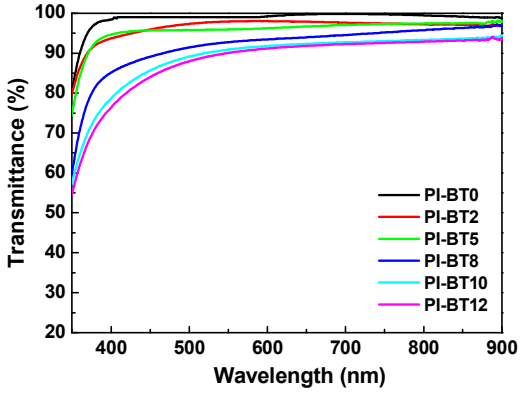

Fig. 4. Optical transmittance spectra of **PI-BTX** hybrid nanocomposite thin films.

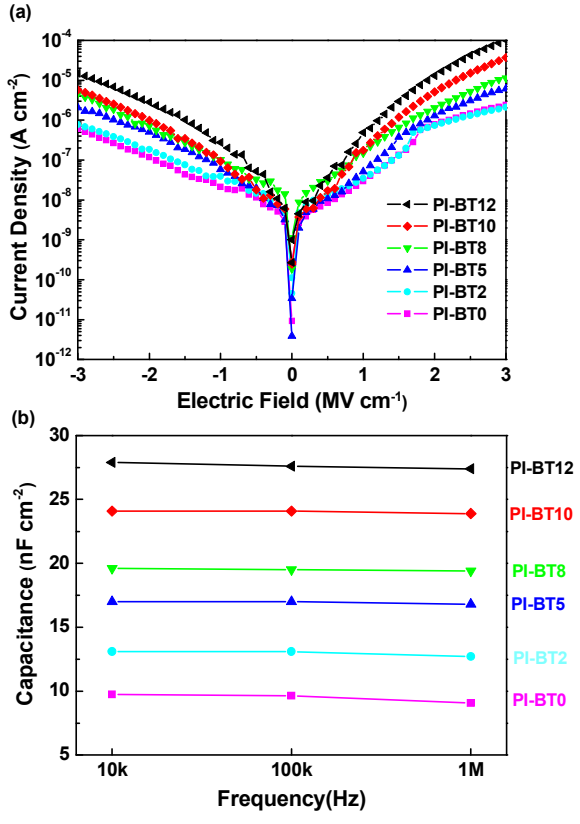

Fig. 5. (a) Leakage characteristics and (b) capacitance vs. frequency plots for the **PI-BTX** hybrid dielectrics.

Table 1. Summary of dielectric and film properties for **PI-BTX** hybrid dielectric film.

dielectric materials	thickness [nm]	T_d [°C]	T_g [°C]	water contact angle [°]	diidomethane contact angle [°]	surface energy [mJ m^{-2}]	RMS roughness [nm]
PI-BT0	351	410	280	63.4	31.1	48.1	0.475
PI-BT2	360	439	302	63.6	31.3	48.0	4.147
PI-BT5	362	464	315	64.3	34.2	46.8	6.675
PI-BT8	355	469	326	66.7	37.6	44.8	8.684
PI-BT10	364	482	348	73.7	49.2	37.9	8.943
PI-BT12	358	493	352	83.5	39.8	39.8	11.924

Table 2. Summary of electrical parameters for MIM device and pentacene OTFTs based on different **PI-BTX** hybrid dielectrics.

dielectric materials	leakage current density[a] [A cm^{-2}]	capacitance[b] [nF cm^{-2}]	dielectric constant[b] [-]	μ [cm^2 V^{-1} s^{-1}]	V_t [V]	I_{ON}/I_{OFF} [-]
PI-BT0	1.17×10^{-7}	9.7	3.9	3.95×10^{-2}	-3.4	1.3×10^{5}
PI-BT2	1.85×10^{-7}	13.1	5.2	3.36×10^{-2}	-4.1	1.1×10^{5}
PI-BT5	5.04×10^{-7}	17.0	6.8	5.38×10^{-2}	-3.7	1.5×10^{5}
PI-BT8	7.27×10^{-7}	19.6	8.0	5.43×10^{-2}	-4.1	1.7×10^{5}
PI-BT10	9.89×10^{-7}	24.1	9.8	2.32×10^{-1}	-0.5	1.8×10^{5}
PI-BT12	2.76×10^{-6}	27.9	11.3	6.38×10^{-2}	2.6	6.7×10^{4}

[a]at -2 MV cm^{-2} [b]at 10 kHz

OTFTs Characteristics with PI-BTX hybrids as dielectric

The dielectric properties of the **PI-BTX** films are strongly dependent on BT content. The MIM capacitor device used for quantitative leakage current/capacitance measurements (Fig. 5) contains various **PI-BTX** hybrid dielectric layers sandwiched between two Al electrodes. Fig. 5(a) shows leakage current densities for the **PI-BTX** hybrid gate dielectric films fabricated on Si substrate, with various BT contents, as a function of an applied field. At a field strength of -2 MV cm^{-1}, the of **PI-BTX** hybrid film leakage current densities are in the range of 1.85×10^{-7}~2.76×10^{-6} A cm^{-2}, slightly greater than that for pure PI film (1.17×10^{-7} A cm^{-2}). Thus, the dielectric properties of these hybrid insulators are suitable for the fabrication of highly stable OTFTs. Fig. 5(b) shows a capacitance (*C*)-frequency (*F*) plot for a MIM structure fabricated using **PI-BTX** dielectrics, for various BT loadings. The figure reveals that increasing BT content effectively enhances the hybrid film's capacitance for a given dielectric thickness. **PI-BTX** hybrid capacitances in the range of 13.1~27.9 nF cm^{-2} at 10 kHz are readily obtainable, and are much greater than the capacitances of a 350 nm-thick SiO_2 layer or of pure PI (**PI-BT0**) film (~9.7 nF cm^{-1}). An observed linear correlation between BT loading and frequency response was flat over the range 10 kHz~1 MHz. At lower frequencies, the capacitance increases slightly, possibly because of increases in the response time available for polarization. The dielectric constants (*k*) were evaluated using the following equation:

$$C = \frac{k\varepsilon_0 A}{d} \quad (1)$$

Where, *C* is the measured capacitance, ε_0 is the permittivity of free space, *A* is the area of the capacitance, and d is the thickness of dielectric layer. Table 2 summarizes the dielectric constants detected at 10 kHz. The measured dielectric constant values for the hybrid materials ranged from 3.9 for **PI-BT0** to 5.2, 6.8, 8.0, 9.8, and 11.3 for **PI-BT2, PI-BT5, PI-BT8, PI-BT10**, and **PI-BT12**, respectively. The dielectric constant for the hybrid dielectric at 12 wt% is about three times that of pristine **PI-BT0**, but it does not induce strong phase separation. The hybrid materials' dielectric constant can be raised by increasing the inorganic BT NPs content; the dielectric constant increases with BT NPs content, because of the higher dielectric permittivity of the well-dispersed nanofiller, isolated by the passivating layers of polymer matrix. The BT NPs present in the PI precursor solution undergo a condensation reaction to form the -O-BT-O- network interface that sterically hinders the movement of BT NPs, resulting in the uniform incorporation of BT NPs in the PI phase. The use of this high dielectric constant inorganic nanomaterial within the PI film affords a greater charge density at the interface, and a smooth surface morphology that minimizes current leakage, facilitated by use of sufficiently thick insulators.

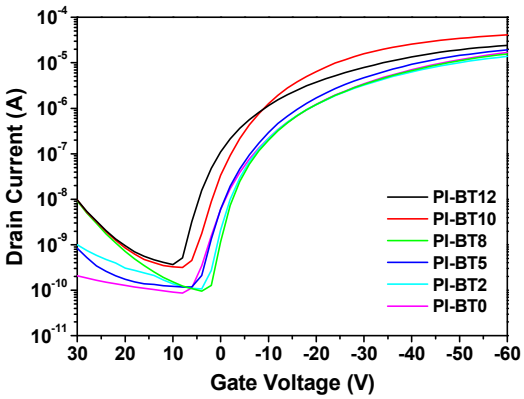

Fig. 6. Transfer characteristics of OTFTs based on various **PI-BTX** hybrid dielectric layers.

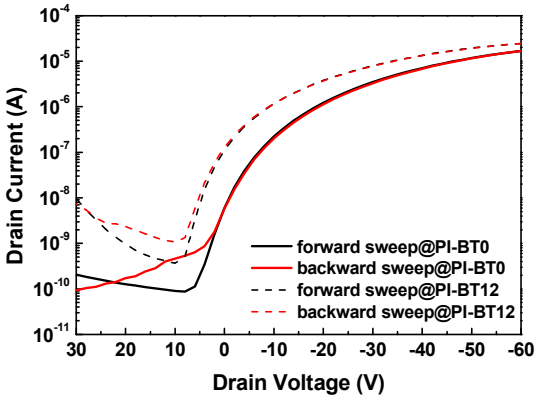

Fig. 7. Dual sweep (forward and backward sweep) transfer characteristics of OTFTs based on **PI-BT0** and **PI-BT12** hybrid dielectric layers.

Thus, we prepared hybrid films for OTFTs applications, while exercising control over the film's dielectric constant.

BGTC pentacene OTFTs were fabricated, using **PI-BTX** hybrid films as the gate dielectric. From the accumulated-mode output plots (Fig. S4 of ESI†), all the devices exhibit typical p-type OTFTs behaviors, suggesting that the majority of transporting carriers in the channel are holes. We determined the field-effect mobility (μ) from the transfer curves, by applying the Equation (2) to the saturation region.

$$I_d = \frac{WC_i}{2L}\mu(V_g - V_t)^2 \qquad (2)$$

Where, I_d is the drain current, V_t is threshold voltage, W and L are the channel width and length respectively, and C_i is the capacitance per unit area of the hybrid gate dielectric. The average field-effect mobility is calculated by plotting the square root of I_d against V_g. Fig. 6 shows a representative transfer plot for OTFTs fabricated using **PI-BTX** as the dielectric. The OTFTs performance characteristics for these devices as a function of BT concentration are collected in Table 2. All of these hybrid dielectrics films are quite smooth, and thus device performance is both reproducible and reliable. Devices using the neat polyimide dielectric, **PI-BT0**, have a hole mobility of 3.95×10^{-2} cm^2 V^{-1} s^{-1}, which approaches previously reported values for pentacene-based OTFTs with other PI materials, and that reported for use of conventional SiO_2 as the gate dielectric.[44-47] Greater hole mobility is obtainable for OTFTs with a larger BT loading concentration, mainly because of increased capacitance, which facilitates the accumulation of charge carriers in the channel. Here, the **PI-BT10** dielectric provides the greatest observed mobility of 2.32×10^{-1} cm^2 V^{-1} s^{-1}. However, an excess of BT sites disrupt the deposition of pentacene, as seen for the **PI-BT12** dielectric based device. Relatively high OTFTs ON/OFF current ratios, of approximately 10^5 are observed for all samples. Interestingly, all the threshold voltages are quite small, even for the neat PIs and samples with low BT loadings; however, **PI-BT12** devices exhibit a more positive threshold voltage. The use of large capacitance hybrid dielectrics is beneficial for reducing threshold voltage, even to a threshold voltage of 0 V, compared to transistor fabricated OTFTs using SiO_2 with a similar thickness. The threshold voltages of OTFTs with **PI-BTX** hybrid dielectrics are not significantly altered; it is possible that the prepared hybrid dielectric can annihilate major charge traps during the condensation reaction process. Compared with the **PI-BT0** dielectric, the electrical hysteresis behavior of **PI-BT12** shows a small change when the gate voltage is swept continuously from 20 to -60 V and then returned to 20 V (Fig. 7). The small hysteresis arises from the unreacted hydroxyl groups that remain in the hybrid gate dielectric.[53] In general, OTFTs exhibit moderately high mobility (>10^{-1} cm^2 V^{-1} s^{-1}), have an acceptable ON/OFF current ratio of approximately 10^5, and operate at low threshold voltages, close to 0 V, if the hybrid dielectric capacitance is increased by incorporating BT at concentrations up to 10 wt%.

Fig. S5 and S6 of ESI† show contact angle measurements for the surfaces of the **PI-BTX** hybrid dielectric materials. We quantified the surface energies of the hybrid gate dielectric by calculation, based on the different polarities of deionized (DI) water and diiodomethane.[54] Table 1 shows contact angle data and surface energies for the **PI-BTX** hybrid dielectrics. A low contact angle at the solid surface contact with a water drop means that the surface is hydrophilic with a large surface energy, while a large contact angle suggests a hydrophobic surface with low surface energy.[54] The **PI-BT0** polymeric film, which lacks added BT, exhibits a small water contact angle of 63.4°. However, hybrid gate dielectrics that incorporated BT show increasing contact angles as the BT content increases. We explain this observation by the fewer hydroxyl groups that are present at greater BT concentrations, because of the condensation reaction between functional PI and the modified BT NPs. Our results also confirm that surface energy reduces to

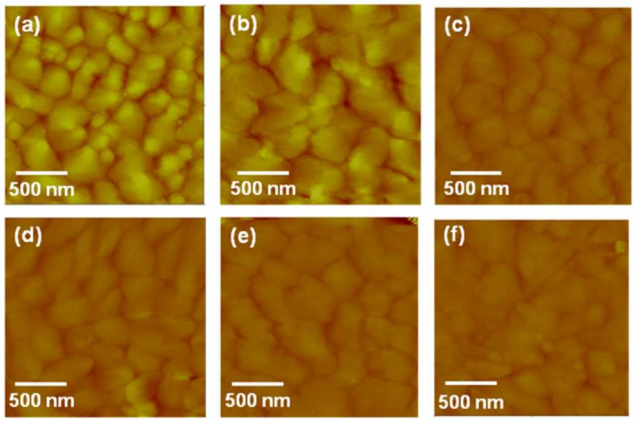

Fig. 8. AFM images of pentacene deposited on dielectric: (a) **PI-BT0**, (b) **PI-BT2**, (c) **PI-BT4**, (d) **PI-BT8**, (e) **PI-BT10**, and (f) **PI-BT12.**

37.9 mJ m^{-2} upon in the presence of 10 wt% BT. High dielectric constant BT NPs are surrounded by the low dielectric constant PI matrix, which reduces the NPs surface energy. In most cases, a dielectric surface with low surface energy and high water contact angle provides sites for organic semiconductor chain growth.[55]

We characterized the morphologies of pentacene thin films grown on **PI-BTX** hybrid dielectrics by AFM (Fig. 8). Pentacene is inherently hydrophobic, and the **PI-BT10** insulator is better matched to the pentacene surface energy and is generally compatible with pentacene growth. The size of pentacene grain domains deposited on hybrid dielectrics increases with BT content in the **PI-BTX** hybrids, thus, the affinity of the dielectric surface for pentacene determines the semiconductor growth rates, and the BT mobility within the OTFTs device (Tables 1 and 2).[56] Reductions in grain size or in the grain boundary between crystallites correlate with the numbers of interfacial trapping sites that may disrupt charge transport. Grain size and charge mobility increase with BT content, from **PI-BT0** to **PI-BT10**. The enhanced mobility observed in pentacene OTFTs based on the **PI-BT10** dielectric demonstrate an efficient charge transport process, because of well-connected domains, without significant charge hopping across grain boundaries and without disordered domains. Insertion of the high dielectric constant hybrid film induces the formation of greater charge carrier densities at the dielectric/semiconductor interface, and thus, improves OTFTs performance because of the resulting improvements in mobility and threshold voltage. However, as the concentration of BT content increases further to 12 wt%, device mobility falls. The rougher morphology of the **PI-BT12** surface, with its aggregates of BT particles, features traps close to the interface, causing significant interference with the formation of crystalline structures. The greater boundary concentration of small aggregated domains in **PI-BT12** restricts charge transport in the semiconductor channel.

In this study, nanocomposite dielectrics composed of PI, with a large fraction of homogenously dispersed large dielectric constant surface-functionalized BT NPs are compared to previously reported direct PI blended nanocomposite materials that do not contain any reactive sites for NPs in their PI matrices.[40-42] Our solution-processable hybrid dielectrics produce improved OTFTs characteristics because of an optimized combination of high dielectric constant inorganic oxide NPs and host PI matrix.

Conclusions

In conclusion, a series of novel high dielectric constant **PI-BTX** hybrid thin films with different inorganic loadings were successfully fabricated for use as a dielectric material in OTFTs. The polymer-inorganic hybrid materials featured a covalently bonded interface, and revealed a high degree of dispersion of BT NPs in the PI matrix. The dielectric constant for the composite material was tunable by varying the weight percent of BT NPs incorporated into the PI matrix, and provided significant improvements in the dielectric properties. The device performance (mobility and threshold voltage), and film properties (dielectric constant, morphology, and hydrophilicity/hydrophobicity) showed a strong correlation with BT concentration. These findings suggest that **PI-BTX** hybrid films can be tailored to meet the requirements of practical applications. Additionally, our PI hybrid materials illustrate a new approach towards the development of transparent, high thermal stability, and environmental safe gate dielectrics for application in the field of transistors and related electronic devices.

Acknowledgements

The authors gratefully acknowledge the financial support provided by the Ministry of Science and Technology of Taiwan.

References

1 S. Allard, M. Forster, B. Souharce, H. Thiem and U. Scherf, *Angew. Chem. Int. Ed.*, 2008, 47, 4070.
2 H. Dong, L. Jiang and W. Hu, *Phys. Chem. Chem. Phys.*, 2011, **13**, 6286.
3 Y. Guo, G. Yu and Y. Liu, *Adv. Mater.*, 2010, **22**, 4427.
4 H. N. Tsao and K. Müllen, *Chem. Soc. Rev.*, 2010, **39**, 2372.
5 A. Facchetti, *Chem. Mater.*, 2011, 23, 733.
6 J. Sun, B. Zhang and H. E. Katz, *Adv. Funct. Mater.*, 2011, **21**, 29.
7 C.-a. Dai, F. Zhang and D. Zhu, *Adv. Mater.*, 2013, **25**, 313.
8 A. R. Murphy and J. M. J. Fréchet, *Chem. Rev.*, 2007, **107**, 1066.
9 C. Wang, H. Dong, W. Hu, Y. Liu and D. Zhu, *Chem. Rev.*, 2012, **112**, 2208.
10 J. Mei, Y. Diao, A. L. Appleton, L. Fang and Z. Bao, *J. Am. Chem. Soc.*, 2013, **135**, 6724.
11 S. Liu, W. M. Wang, A. L. Briseno, S. C. B. Mannsfeld, Z. Bao, *Adv. Mater.*, 2009, **21**, 1217.
12 A. A. Virkar, S. Mannsfeld, Z. Bao and N. Stingelin, *Adv. Mater.*, 2010, **22**, 3857.
13 Y. Wen, Y. Liu, Y. Guo, G. Yu and W. Hu, *Chem. Rev.*, 2011, 111, 3358.
14 Y. D. Park, J. A. Lim, H. S. Lee and K. Cho, *Mater. Today*, 2007, **10**, 46.
15 S. A. DiBenedetto, A. Facchetti, M. A. Ratner and T. J. Marks, *Adv. Mater.*, 2009, **21**, 1407
16 C.-a. Dai, Y. Liu, G. Yu and D. Zhu, *Acc. Chem. Res.*, 2009, **42**, 1573.
17 H. Wang and D. Yan, *NPG Asia Mater.*, 2010, **2**, 69.
18 H. Ma, O. Acton, D. O. Hutchins, N. Cernetic and A. K.-Y. Jen, *Phys. Chem. Chem. Phys.*, 2012, **14**, 14110.
19 J. Veres, S. Ogier and G. Lloyd, *Chem. Mater.*, 2004, **16**, 4543.
20 A. Facchetti, M.-H. Yoon and T. J. Marks, *Adv. Mater.*, 2005, **17**, 1705.
21 R. P. Ortiz, A. Facchetti and T. J. Marks, *Chem. Rev.*, 2010, **110**, 205.
22 S. Gross, D. Camozzo, V. D. Noto, L. Armelao and E. Tondello, *Euro. Polym. J.*, 2007, **43**, 673.
23 F.-C. Chen, C.-W. Chu, J. He, Y. Yang and J.-L. Lin, *Appl. Phys. Lett.*, 2004, **85**, 3295.
24 S. Jeong, D. Kim, S. Lee, B.-K. Park and J. Moon, *Appl. Phys. Lett.,* 2006, **89**, 092101.
25 C. Jung, A. Maliakai, A. Sidorenko and T. Siegrist, *Appl. Phys. Lett.*, 2007, 90, 062111.
26 S. Jeong, S. Lee, D. Kim, H. Shin and J. Moon, *J. Phys.*

Chem. C, 2007, **111**, 16083.
27 S. Jeong, D. Kim and J. Moon, *J. Phys. Chem. C*, 2008, **112**, 5245.
28 S. Lee, S. Jeong and J. Moon, *Org. Electron.*, 2009, **10**, 982.
29 Y. Gan, Q. J. Cai, C. M. Li, H. B. Yang, Z. S. Lu, C. Gong and M. B. Chan-Park, *ACS Appl. Mater. Interface*, 2009, **1**, 2230.
30 Y.-g. Ha, S. Jeong, J. Wu, M.-G. Kim, V. P. Dravid, A. Facchetti and T. J. Marks, *J. Am. Chem. Soc.*, 2010, **132**, 17426.
31 J. Kim, S. H. Lim and Y. S. Kim, *J. Am. Chem. Soc.*, 2010, **132**, 14721.
32 L. Li, W. Hu, L. Chi and H. Fuchs, *J. Phys. Chem. B.*, 2010, **114**, 5315.
33 N. T. Tien, T. Q. Trung, Y. G. Seoul, D. I. Kim and N.-E. Lee, *ACS Nano*, 2011, **5**, 7069.
34 Y. Wang and H. Kim, *Org. Electron.*, 2012, 13, 2997.
35 Y. Zhou, S.-T. Han, Z.-X. Xu and V. A. L. Roy, *J. Mater. Chem.*, 2012, **22**, 4060.
36 Y. Zhou, S.-T. Han, Z.-X. Xu, X.-B. Yang, H.-P. Ng, L.-B. Huang and V. A. L. Roy, *J. Mater. Chem.*, 2012, *22*, 14246.
37 R. Schroeder, L. A. Majewski and M. Grell, *Adv. Mater.*, 2005, **17**, 1535.
38 P. Kim, S. C. Jones, P. J. Hotchkiss, J. N. Haddock, B. Kippelen, S. R. Marder and J. W. Perry, *Adv. Mater.*, 2007, **19**, 1001.
39 P. Kim, X. H. Zhang, B. Domercq, S. C. Jones, P. J. Hotchkiss, S. R. Marder, B. Kippelen and J. Perry, *Appl. Phys. Lett.*, 2008, **93**, 013302.
40 W.-H. Lee, C. C. Wang, W.-T. Chen and J.-C. Ho, *Jpn. J. Appl. Phys.*, 2008, **47**, 8955.
41 W.-H. Lee and C. C. Wang, *J. Vac. Sci. Technol. B*, 2009, **27**, 1116.
42 W.-H. Lee, C. C. Wang and S. D. Liu, *J. Nanosci. Nanotech.*, 2011, **11**, 1968.
43 L. H. Chen, P. Lin, J. C. Ho, C. C. Lee, C. Kim and M. C. *Chen, Synth. Met.*, 2011, **161**, 1527.
44 Y. Kato, S. Iba, R. Teramoto, T. Sekitani, T. Someya, H. Kawaguchi and T. Sakurai, *Appl. Phys. Lett.*, 2004, 84, 3789.
45 S. Y. Yang, S. H. Kim, K. Shin, H. Jeon and C. E. Park, *Appl. Phys. Lett.*, 2006, **88**, 173507.
46 S. Pyo, Y. Lee, J. Jeon, M. H. Yi and S.-K. Kwon, *J. Appl. Phys.*, 2006, **99**, 073711.
47 T. Sekitani, T. Someya and T. Sakurai, *J. Appl. Phys.*, 2006, **100**, 024513.
48 G.-S. Liou, P.-H. Lin, H.-J. Yen, Y.-Y. Yu and W.-C. Chen, *J. Polym. Sci. Polym. Chem.*, 2010, **48**, 1433.
49 G.-S. Liou, P.-H. Lin, H.-J. Yen, Y.-Y. Yu, T.-W. Tsai and W.-C. Chen, *J. Mater. Chem.*, 2010, **20**, 531.
50 V. Torres-Heredia, J. Muñoz-Saldaña, F. J. Espinoza Beltrán, A. Márquez Herrera and A. Zapata Navarro, *Adv. in Tech. of Mat. and Mat. Proc. J.*, 2005, **7**, 105.
51 S. H. Choi, I. D. Kim, J. M. Hong, K. H. Park and S. G. Oh, *Mater. Lett.*, 2007, **61**, 2478.
52 Y.-W. Wang and W.-C Chen, *Mater. Chem. Phys.*, 2011, **126**, 24.
53 S. Lee, B. Koo, J. Shin, E. Lee, H. Park and H. Kim, *Appl. Phys. Lett.*, 2006, **88**, 162109.
54 A. J. Kinloch, *Adhesion and adhesives: science and technology, Chapman & Hall*, 1987, pp 24-38.
55 W. Y. Chou, C.-W. Kuo, H.-L. Cheng, Y.-R. Chen, F.-C. Tang, F.-Y. Yang, D.-Y. Shu and C.-C. Liao, *Appl. Phys. Lett.*, 2006, **89**, 112126.
56 C. Kim, A. Facchetti and T. J. Marks, *Science*, 2007, **318**, 76.

Table of contents entry

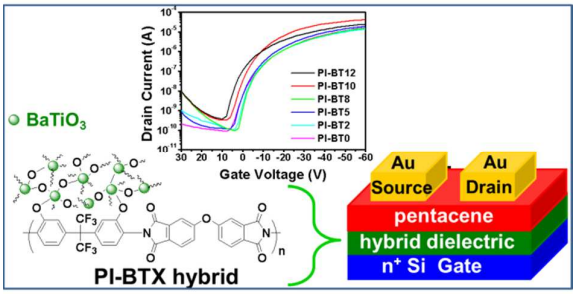

Polyimide (PI)-$BaTiO_3$ (BT) NPs hybrid nanocomposite dielectrics with tunable BT loadings (X) were fabricated for investigating the properties on the pentacene organic thin film transistors (OTFTs).